Journal of Power Sources 273 (2015) 999–1005

Contents lists available at ScienceDirect

Journal of Power Sources

journal homepage: www.elsevier.com/locate/jpowsour

# Co-extrusion of electrolyte/anode functional layer/anode triple-layer ceramic hollow fibres for micro-tubular solid oxide fuel cells–electrochemical performance study

Tao Li, Zhentao Wu, K. Li*

*Department of Chemical Engineering, Imperial College London, London SW7 2AZ, UK*

## HIGHLIGHTS

- Single-step fabrication of triple-layer ceramic hollow fibres with controllable morphologies.
- The fibres comprises electrolyte, anodic functional layer (AFL) and anode layer.
- Uniform AFL allows systematic investigations of its roles in cell performances.
- Time and cost effective fabricating technique is suitable for larger-scaled productions.

## ARTICLE INFO

*Article history:*
Received 9 May 2014
Received in revised form
12 September 2014
Accepted 1 October 2014
Available online 7 October 2014

*Keywords:*
AFL
Co-extrusion/co-sintering
Hollow fibre
Micro-tubular SOFC

## ABSTRACT

In this study, the effects of an anode functional layer (AFL) with controlled thickness on physical and electrochemical properties of a micro-tubular SOFC have been systematically studied. A series of electrolyte/AFL/anode triple-layer hollow fibres with controllable AFL thicknesses (16.9–52.7 μm) have been fabricated via a single-step phase-inversion assisted co-extrusion technique. Both robustness of the cell and gas-tightness of the electrolyte layer are considerably improved by introducing the AFL of this type. The fracture force of the sample with the thickest AFL (9.67 N) almost doubles when compared to the electrolyte/anode dual-layer counterpart (5.24 N). Gas-tightness of the electrolyte layer is also considerably increased as AFL contributes to better-matched sintering behaviours between different components. Moreover, the formation of an AFL simultaneously with electrolyte and anode significantly improves the cell performances. The sample with the thinnest AFL (approximately 16.9 μm, 6% of the total anode thickness) leads to a 30% (from 0.89 to 1.21 W $cm^{-2}$) increase in maximum power density, due to increased triple-phase boundaries (TPB). However, further increase in TPB from a thicker AFL is less effective for improving the cell performance, due to the substantially increased fuel diffusion resistance and subsequently higher concentration polarization. This indicates that the control over the AFL thickness is critically important in avoiding offsetting the benefits of extended TPB and consequently decreased cell performances.



## 1. Introduction

Solid oxide fuel cells (SOFCs) have received considerable research attentions as one of the most promising technologies for sustainable energy generation in the future. The high working temperatures (850–1000 °C) result in high-quality excess heat, which can be further used to drive additional gas turbines or be stored in medium, thus leading to very high system efficiency [1–3]. The planar geometric design, which received probably the most interest, has been successfully commercialized in, for example, domestic combined heat and power (CHP) system and auxiliary power units (APUs). The micro-tubular design, which was first reported in 1990s, has attracted an increasing level of interest by exhibiting a number of desirable characteristics, such as high volumetric power density, superior thermal shock resistance and rapid start-up/shut down [4,5]. However, there exist several challenges, such as a limited range of appropriate materials due to high working temperatures, and a lack of cost-effective manufacturing routes, which prohibit its development from early lab-scale research to commercially viable products. Therefore, there is a

* Corresponding author. Tel.: +44 207 5945676; fax: +44 207 5945629.
*E-mail address:* Kang.Li@imperial.ac.uk (K. Li).

http://dx.doi.org/10.1016/j.jpowsour.2014.10.004
0378-7753/

need to reduce the working temperature to the so-called intermediate range (500–750 °C), as defined by Steele [6], and to apply new technologies for a more economical fabrication process.

Lowering the working temperature to the intermediate temperature range markedly extends the range of available materials, which to some extent allows cheaper fabrication, interconnects and balance-of-plant (BoP) components in particular [7]. Another benefit from lowering the working temperature is a further decrease in the start-up/shut-down time, which makes this desirable advantage of micro-tubular geometric design more prominent. Co-extrusion technique was first applied in polymeric membrane systems in 1980s for more straightforward and economic fabrication [8,9]. However, in terms of ceramic membrane system, there exist other concerns such as mismatch between rheological properties during spinning and shrinking behaviours during sintering. It was not until recent years when co-extrusion has been adopted in fabricating multi-layer micro-tubes for SOFC applications [10–15]. This technique has illustrated a number of desired characteristics over conventional multi-step processes which comprise repetitions of coating and sintering, such as great process control, better tailoring over morphologies and reduced fabrication costs. Moreover, this technique enables better adhesion between cell components, leading to a reduced ohmic loss and contact resistance. Therefore, co-extrusion has the potential to become a reliable and economical technique for mass-scale production.

The feasibility of using a phase-inversion assisted co-extrusion technique to fabricate triple-layer ceramic hollow fibre has been previously proved [16]. In this study, a more controllable fabrication has been realized and the effects of AFL thicknesses on electrochemical performances have been systemically investigated. The triple-layer structure includes anode, electrolyte and an anode functional layer (AFL) between them. The benefits of employing an AFL have been well proved and accepted, such as to introduce a gradient in conductivity and shrinkage behaviours, as well as to enlarge the triple phase boundary (TPB) by the fine structure and subsequently improve the performance of micro-tubular SOFCs. On the other hand, the reduced porosity in this fine structure also tends to introduce considerable resistance towards the transport of fuel gases and subsequently increase the concentration polarization [17,18]. In previous studies, a thicker AFL was normally obtained by a second coating process, forming an interface inside AFL [18,19]. This can lead to additional issues such as problematic adhesion between layers and increased resistance at the interface between multiple coatings, which subsequently offset the benefits from introducing a thicker AFL. In this study, the one-step co-extrusion technique enables the fabrication of 'interface-free' AFL when adjusting the thicknesses, which enables the effects of a wider range of AFL thicknesses to be investigated in a more systematic way.

## 2. Experimental

### 2.1. Materials

Cerium–gadolinium oxide ($Ce_{0.9}Gd_{0.1}O_{1.95}$ (CGO), with surface area 30–40 $m^2\ g^{-1}$, mean particle size (d50) 0.1–0.4 μm), nickel oxide (surface area 3–7 $m^2\ g^{-1}$, mean particle size (d50) 0.5–1.5 μm) and lanthanum strontium cobalt ferrite ($La_{0.6}Sr_{0.4}Co_{0.2}Fe_{0.8}O_3$ (LSCF), surface area 11.79 $m^2\ g^{-1}$) are commercially available from NexTech Materials Ltd. (Ohio), and they were used as supplied. N-methyl-2-pyrrolidone (NMP), ethanol and dimethyl sulfoxide (DMSO) (99%+, VWR International, LLC) were used as solvent. Polyethersulfone (PESf) purchased from Radel A-300, Ameco Performance (USA) and Polyethyleneglycol 30-dipolyhydroxystearate (Arlacel P135, Uniqema) were used as the polymer binder and the dispersant of the spinning suspensions, respectively. During the spinning, de-ionized water and tap water were adopted as the internal and external coagulants, respectively.

### 2.2. Fabrication of anode/AFL/electrolyte triple-layer hollow fibres

Details of the co-extrusion based single-step fabrication process have been described elsewhere [16]. Three spinning suspensions were first prepared. The CGO/NiO ratios in anode and AFL suspensions were 2:3 and 3:2, respectively. Previous research has suggested that using a mixture of NMP and ethanol as the solvent could provide anode morphology facilitating fuel transport [12,20]. Therefore, NMP containing 5% ethanol was used as solvent for anode suspension and DMSO was used as the solvent for AFL and electrolyte suspensions. The ceramic powders were first mixed with solvent and dispersant and stirred on a roll miller for 3–4 days to disperse powders uniformly. The polymer binder (10% of the total weight of ceramic powders) was subsequently added into the mixture and a further mixing of 4–5 days was undertaken to dissolve the polymer and guarantee the homogeneity of spinning suspensions. Prior to the co-extrusion process, a degassing process was conducted at room temperature, during which all three spinning suspensions were positioned in a vacuum chamber under stirring to remove trapped air bubbles which may disrupt the continuity of spinning. After degassing, precursor fibres were fabricated via a phase-inversion based co-extrusion technique, in which all components were simultaneously extruded through a custom-designed quadruple-orifice spinneret, as illustrated in Fig. 1. The extrusion rates of each component were accurately controlled by syringe pumps (Harvard PHD22/200 HPsi and KDS410). Detailed compositions of three spinning suspensions and their corresponding extrusion rates adopted during spinning are summarized in Table 1.

The co-sintering was undertaken at 1500 °C for 12 h using a tubular furnace (CARBOLITE) after triple-layer precursor fibres were cut to a certain length (~15 cm) and dried at room temperature, and the three-step sintering profile was described elsewhere [11]. For some post-sintering characterizations, the co-sintered triple-layer hollow fibres need to be reduced, converting NiO into Ni. The reduction was conducted at 550 °C in pure hydrogen atmosphere for 2.5 h.

### 2.3. Characterizations

Scanning electron microscopy (SEM) (JEOL JSM-5610 LV) was applied to study the morphology for both precursors and sintered fibres. A clean cross section was obtained by flexing the fibres until a fracture occurred and samples were subsequently placed vertically on a metal holder. Prior to the observation, a gold-coating was applied under vacuum for 1.5 min at 20 mA (EMITECHModel K550). Both secondary electrons imaging (SEI) and backscattered electrons (BSE) modes were adopted to obtain high-resolution images at varying magnifications.

The mechanical strength of the hollow fibres was investigated via a three-point bending method using a tensile tester (Instron Model 5544) with a 5 kN load cell. Prior to the measurement, hollow fibres were reduced at 550 °C, converting NiO into Ni. Fibre samples were positioned onto a sample holder with a distance of 30 mm. The bending strength ($\sigma_F$) was calculated based on the following equation [21]:

$$\sigma_F = \frac{8FLD_o}{\pi\left(D_o^4 - D_i^4\right)} \quad (1)$$

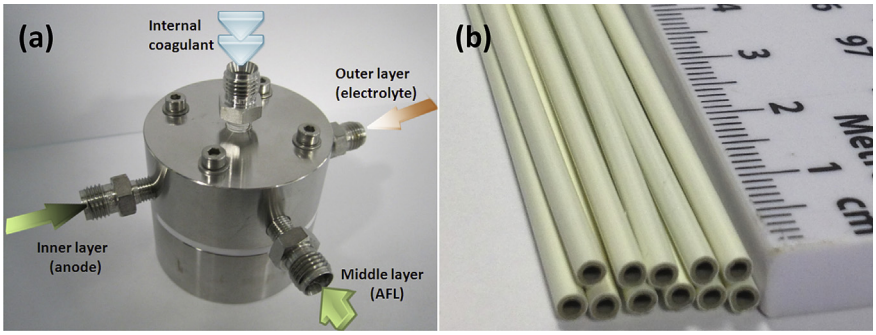


**Fig. 1.** Photographic pictures of (a) quadruple-orifice spinneret; (b) example of triple-layer precursors.

where $F$ denotes the measured force when a fracture occurs; $L$, $D_o$ and $D_i$ represent fibre length (in this case, 30 mm), the outer and inner diameters of the fibre, respectively.

The gas-tightness property of electrolyte was investigated using a $N_2$ permeation method described elsewhere [22]. The $N_2$ permeance was calculated based on the pressure change over a certain period of time (8 h).

$$P = \frac{V}{RT \times A_m t} \ln\left(\frac{p_0 - p_a}{p_t - p_a}\right) \quad (2)$$

$$A_m = [2\pi(R_o - R_{in})L]/\ln(R_o/R_{in}) \quad (3)$$

where $P$ denotes the $N_2$ permeance of the test membrane (mol $m^{-2}$ $s^{-2}Pa^{-1}$); $V$ is the volume of the test vessel ($m^3$); $R$ is the gas constant (8.314 J $mol^{-1}$ $K^{-1}$); $T$ denotes the measured temperature (K); $p_0$, $p_a$, $p_t$ represent the initial, atmospheric and final pressure readings (Pa), respectively. $A_m$ is the membrane area ($m^2$). $R_o$ and $R_{in}$ denote the outer and inner radiuses of the electrolyte, respectively; $L$ is the length of the fibre and $t$ is the time for the measurement ($s$).

Prior to the performance test, a multi-layer cathode with a length of 10 mm was incorporated on electrolyte surface by dip-coating. The first layer was composed of equal percentage of CGO and LSCF, while the second layer was pure LSCF. The slurry was prepared by mixing ceramic powers with solvent (DMSO) and polymer binder (PESf). The procedure was similar to that of the preparation of spinning suspensions. The dip coating of the second layer was carried out after the first layer was dried. When both layers were dried, a heat treatment at 1200 °C for 5 h was undertaken to obtain a complete single cell with an active cell length of 10 mm. Fig. 2 displays a schematic diagram of the experimental set-up of electrochemical performance test. The single cell was first sealed into two gas-tight alumina tubes (Multi-lab Ltd, UK) using a ceramic sealant (Aremco, Ceramabond 552-VFG) after applying current collectors. The current collection of cathode was achieved by wrapping silver wires on cathode surface and silver paste was adopted to improve the contact between cathode and silver wires. In terms of current collection from anode, silver wires were passed through the lumen, with some additional silver paste to enhance the contact between anode surface and silver wires. Both silver wires from anode and cathode were connected to a potentiostat/galvanostat (Iviumstat, Netherlands) for $I$–$V$ measurement and impedance analysis. These electrochemical performance tests were conducted at 600 °C using 20 ml $min^{-1}$ of humidified hydrogen fed to anode as the fuel and static air as oxidant. Electrochemical impedance spectroscopy (EIS) analysis was undertaken in the frequency range from 100 kHz to 0.01 Hz with signal amplitude of 10 mV under open-circuit conditions. The fuel utilization rate was computed via the equation below:

$$U_f = \frac{I}{2F \times n_{H_2,inlet}} \times 100\% \quad (4)$$

where $I$ denotes the electric current collected from the cell (A); $F$ represents Faraday constant (A s $mol^{-1}$); $n_{H_2,inlet}$ is the molar flow rate of hydrogen (mol $s^{-1}$). In this study, $I$ refers to the current at maximum power density, assuming that the electric current is a linear function of the molar flow of the spent fuel.

**Table 1**
Compositions and co-extrusion parameters of the spinning suspensions for triple-layer hollow fibres.

| Spinning components | Anode (wt.%) | AFL (wt.%) | Electrolyte (wt.%) | Bore fluid ($H_2O$) |
|---|---|---|---|---|
| NiO (wt.%) | 42.0 | 25.4 | / | / |
| CGO (wt.%) | 27.9 | 38.1 | 60.0 | / |
| Polymer binder (wt.%) | 7.00 | 6.35 | 6.00 | / |
| Dispersant (wt.%) | 0.15 | 0.15 | 0.15 | / |
| Solvent (wt.%) | NMP + 5%Ethanol 22.85 | DMSO 30.00 | DMSO33.85 | / |
| Extrusion rates (ml $min^{-1}$) | 7 | 3-0 | 0.8 | 10 |

## 3. Results and discussions

### 3.1. Morphology

As can be seen from Fig. 3(a), the prepared triple-layer hollow fibre displays an asymmetric structure with two typical morphologies formed during phase inversion, namely the finger-like channels and sponge-like structure. Fig. 3(b) displays the cross-sectional SEM image of the triple-layer hollow fibre, in which the two morphologies could be more clearly observed. The finger-like channels occupy approximately 60% of the whole cross-section, with a relatively uniform distribution. Fig. 3(c) shows a close-up image of the electrolyte, which illustrates that the electrolyte has been properly connected to the anode layer, together with good densification, during the co-sintering. The using of backscattered electrons (BSE) mode SEM could display a discernable colour difference between CGO and NiO particles, as described elsewhere [16]. Therefore, layers with different ratios between CGO and NiO can be distinguished from each other, which subsequently helps in measuring the thicknesses of each component (Table 2). As shown in the table, a direct proportional relationship could be obtained between the extrusion rates of AFL and thicknesses, suggesting that a relatively precise control over the thicknesses could be achieved during co-extrusion. Moreover, a higher extrusion of AFL leads to an

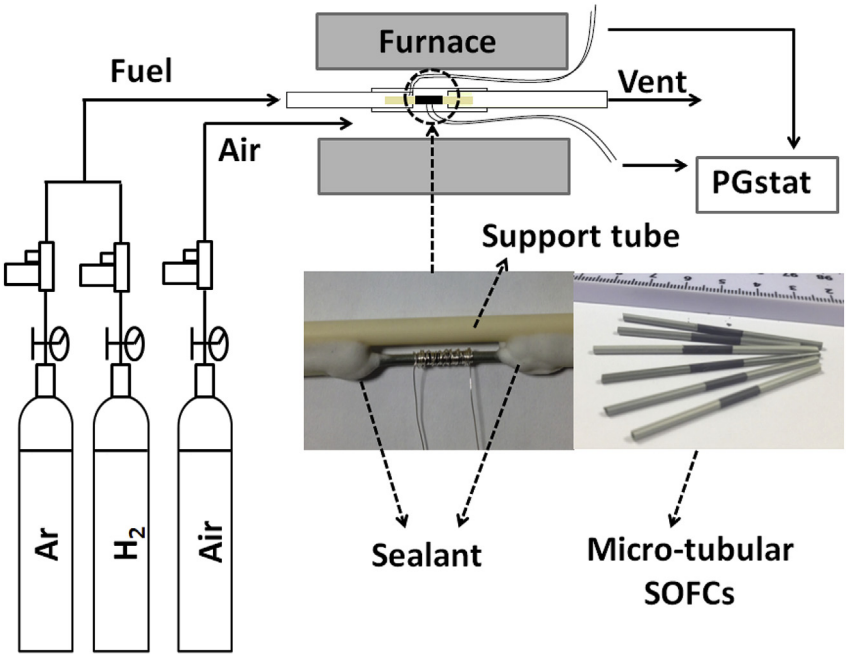


**Fig. 2.** Schematic diagram of the performance test set-up.

increase in the outer diameter of the hollow fibre, while the inner diameter remains almost the same. It is also worth noticing that the thicknesses of electrolyte are relatively constant, which to some extent eliminates the influences of the related ohmic resistance in affecting the cell performances. The obtained results are slightly different from the one in our previous research [16], in which both thicknesses of anode and electrolyte vary as the extrusion rate of AFL changes. This is due to the differences in solid loadings that subsequently affect the rheology of spinning suspensions. For example, in this study, anode suspension has a markedly higher solid loading (70%) compared with the one of AFL (63.5%), making the inner anode layer the major factor that determines the overall velocity during co-extrusion.

The effects of adding ethanol into spinning suspensions on fibre morphologies and properties have been systematically studied in our previous researches [20,23]. An ethanol concentration of 5% is also suggested as an additive to manipulate solvent properties, which has been reported to provide the best performances. NMP is a favourable solvent for phase-inversion assisted extrusion process due to several advantages, such as good mutual affinity with water, high solvent power for polymers, low toxicity and relatively high boiling point. High solubility of polymers in NMP also results in

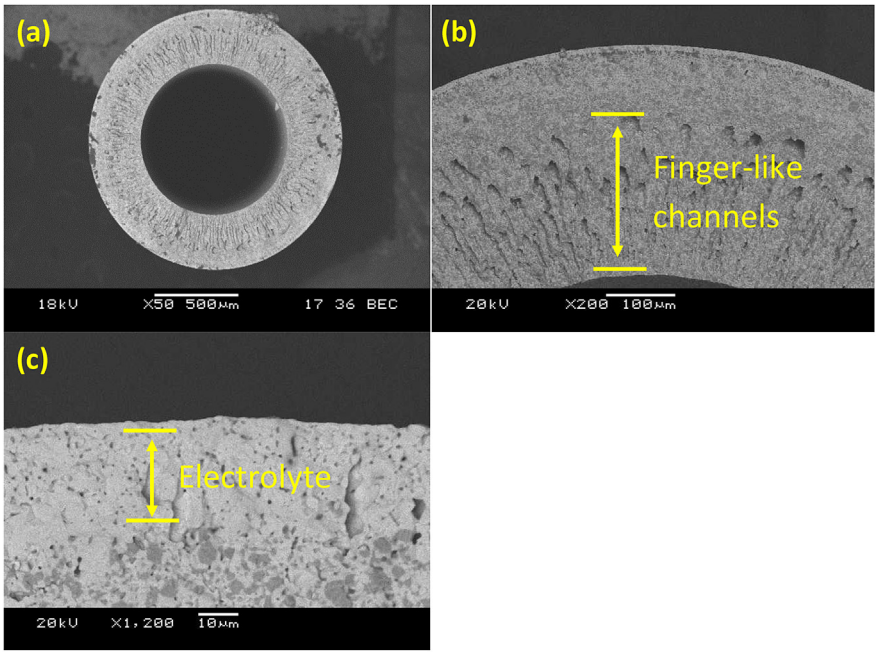


**Fig. 3.** SEM images of the fibre with the AFL extrusion rate of 2 ml $min^{-1}$: (a) overall view, (b) cross-section, (c) electrolyte/electrode interface.

**Table 2**
Dimensions of triple-layer hollow fibres with different extrusion rates of AFL.

| Extrusion rate of AFL (ml $min^{-1}$) | OD (μm) | ID (μm) | Thickness of AFL (μm) | Thickness of anode (μm) | Thickness of electrolyte (μm) |
|---|---|---|---|---|---|
| 0 | 1465.2 | 883.0 | / | 275.8 | 15.3 |
| 1 | 1518.9 | 880.9 | 16.9 | 282.4 | 14.6 |
| 2 | 1540.2 | 878.3 | 32.6 | 284.4 | 13.9 |
| 3 | 1571.3 | 883.7 | 50.7 | 278.9 | 14.2 |

delayed precipitation of polymer binder during phase inversion, which subsequently contributes to long finger-like channels with bigger diameter [23]. However, finger-like channels of this type are undesired due to limited sponge-like structure, which is the major contributor to triple-phase boundary for electrochemical reactions. The introduction of ethanol as a non-solvent shortens the distance between initial polymer solution and the precipitation point, thus accelerating the phase inversion process and resulting in shorter and narrower finger-like channels. Another benefit from NMP-based solvent system is a wider finger entrances at the inner surface. Some previous studies have reported that finger entrance size of NMP & 5% ethanol is more than 1 μm, while the value of DMSO system, which is another widely used solvent, is around 0.7 μm. Li et al. [24] have conducted some theoretical calculations about the effects of pore structure on membrane's coefficient and concluded that the diffusion resistance through the pores could be considered negligible if the pore diameter is larger than 1 μm. This indicates NMP solvent system could help to facilitate the diffusion of gaseous fuels and exhaust gases, which subsequently leads to reduced concentration resistance.

### 3.2. Gas-tightness and mechanical strength

Gas-tightness is an important property, as one of the major functions of electrolyte is to prevent the direct contact between fuel gases and oxidants. In addition, it markedly influences the open circuit voltage (OCV) during electrochemical performance test. In this study, the gas-tightness was investigated via a $N_2$ permeation method and the results are presented in Fig. 4. As can be seen from the graph, the nitrogen permeance of the samples with an AFL is almost one magnitude lower than that of the dual-layer counterpart without an AFL. As introduced in Section 3.1, samples with different AFL extrusion rates have similar electrolyte thickness (Table 2), which indicates that the insertion of an AFL effectively improves the densification of electrolyte by reducing the mismatch in sintering behaviours between different components during co-sintering. This explanation matches well with previous studies [16]. According to Tan's work [22], hollow fibres with its nitrogen permeance at the level of $10^{-10}$ mol $m^{-2}$ $s^{-1}$ $Pa^{-1}$ could be considered to be gas-tight. As shown in the figure, the gas-tightness of all samples with an AFL is located within this range. Therefore, the proper gas-tightness in this study indicates that the fabricated triple-layer hollow fibres are suitable to be constructed into a complete micro-tubular SOFC.

Mechanical strength is essential in determining the lifetime of fuel cells and was investigated using three-point bending method in this study. As shown in Fig. 5, inserting an AFL could effectively improve the robustness of hollow fibres. Both fracture force and bending strength display a proportional relationship with the thickness of AFL due to its full-sponge structure. The fracture force of the sample with the thickest AFL (9.67 N) almost doubles compares with the dual-layer counterpart (5.24 N) without an AFL, while its bending strength shows an increment by around 40% (from 146.7 MPa to 211.7 MPa). This considerable increase in mechanical property may also be explained by that introducing an AFL facilitates the co-sintering process by reducing the mismatch in sintering behaviours between different components. However, the trend in bending strength is slightly different compared with previous study [16], in which the bending strength of samples with the AFL extrusion rates of 1 and 2 ml $min^{-1}$ are lower than the counterpart. This could also be explained by the tailoring of compositions of suspensions, which leads to smaller changes in the fibre dimensions (outer and inner diameter) when the extrusion rate of AFL varies. Some previous studies have suggested that anode-supported hollow fibres with a bending strength of around 150 MPa could be well constructed into a complete single cell [25], which means triple-layer hollow fibres fabricated via co-extrusion are suitable for micro-tubular SOFC application.

### 3.3. Electrochemical performance

Performance test was undertaken at 600 °C with 20 ml $min^{-1}$ of pure hydrogen flowing through anode as the fuel and atmospheric air as oxidant, after coating an LSCF based cathode layer. The active area used to calculate the current density is usually the area of the fuel electrode [26]. As for the micro-tubular structure in this study, in which the anode (fuel electrode) is placed in the lumen side, an active area of 0.276 $cm^2$ was calculated using the inner diameter of the hollow fibres. Fig. 6 illustrates both cell voltages and power

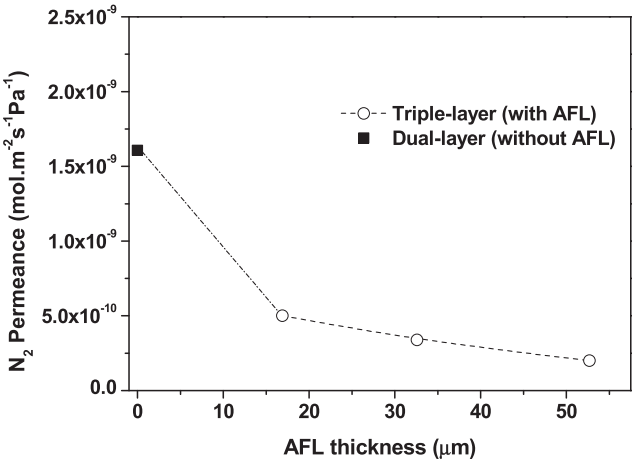


**Fig. 4.** Gas-tightness property as a function of different AFL thicknesses.

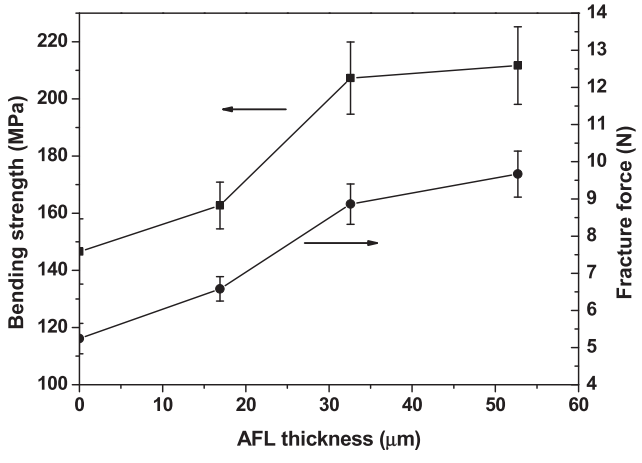


**Fig. 5.** Bending strength and fracture force of reduced samples as a function of different AFL thicknesses (Number of samples = 4).

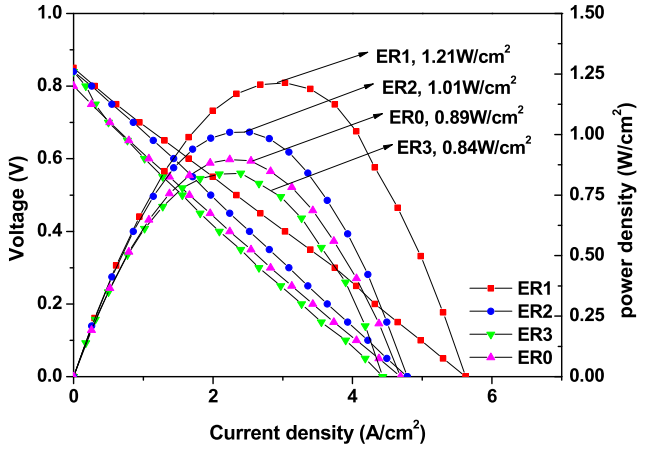


**Fig. 6.** Open-circuit voltage (OCV) and power density as a function of current density of samples with different AFL thickness (ER denotes the extrusion rates of AFL during co-extrusion).

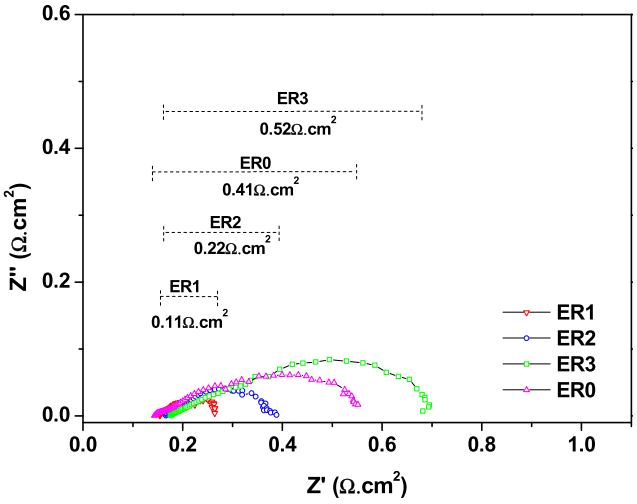


**Fig. 8.** Effects of AFL thickness on SEI analysis of samples under open-circuit condition.

density as a function of current density for micro-tubular single cell prepared from ER1, ER2 and ER3 (ER is the abbreviation of extrusion rate of AFL), while ER0 denotes the dual-layer counterpart without an AFL. As shown in the figure, all samples with an AFL display an open-circuit voltage (OCV) of around 0.85 V at 600 °C, which is slightly higher than the dual-layer counterpart (~0.8 V), due to a better gas-tightness of electrolyte (Fig. 4). The obtained OCV values are lower compared with Nernst Voltage (approximately 1.1 V in this study), which could be due to the formation of reversible electrical conductivity of CGO at 600 °C in reducing atmosphere. This partial reduction from $Ce^{4+}$ to $Ce^{3+}$ leads to the formation of n-type conductivity and then the 'current leakage' between the two electrodes. However, the maximum power densities of 1.21, 1.01, 0.89 and 0.84 W $cm^{-2}$ were obtained for sample ER1, ER2, ER0 and ER3, respectively, which are comparable with other studies [12,27]. In addition, the maximum power density from ER1 shows an increment by 30% when compared with the dual-layer counterpart, which is attributed to the increased in TPB from inserting an AFL and subsequently enlarged reactive sites for electrochemical reactions. This is also in line with some previous studies [19,28].However, the power density shows an inverse proportional relationship with the thicknesses of AFL. Sample ER3 with the thickest AFL (~53 μm) even exhibits lower power density compared

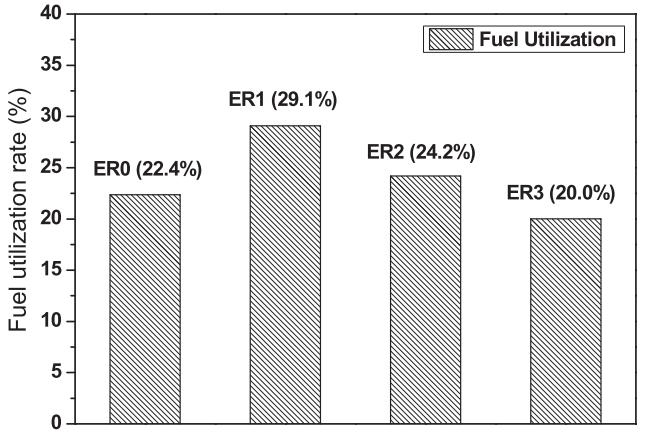


**Fig. 7.** Fuel utilization rates of samples with different AFL thicknesses. The values were calculated via Eq. (3) using the current value at the maximum power density of each cell.

to the dual-layer counterpart, suggesting that introducing an AFL leads to a trade-off effect between enlarging TPB and increasing gas transport resistance. Fuel utilization rates were computed using the current values at the maximum power density of each cell and the obtained trend, as shown in Fig. 7, matches well with the power density results. The sample with the thinnest AFL displays the highest fuel utilization rate (29.1%). So far, sample with AFL thickness of approximately 17 μm (6% of anode thickness) has shown the highest power density and fuel utilization rate.

This explanation could be further proved by the EIS (electrochemical impedance spectroscopy) analysis, as shown in Fig. 8. The first intercept on the real resistance axis (*X* axis) denotes the value of ohmic area specific resistance (ASR), which is composed of the internal resistances of electrolyte and electrodes, and contact resistances between different components. It can be observed that samples with AFL display slightly higher ohmic resistance than the dual-layer counterpart, which could be due to the additional resistance introduced from AFL. As described in Table 2, the thicknesses of anode and electrolyte maintain relatively constant when the extrusion rate of AFL varies. Moreover, the fabrication condition of cathode is almost identical. Therefore, it is reasonable to assume that differences from electrolyte, anode and cathode are considered negligible. The span length between the two intercepts with *X*-axis represents the polarization resistance, which mainly includes concentration polarization and activation polarization. The former one is caused by mass transport resistance through electrodes and interfaces, while the latter one is associated to TPB and the number of reactive sites. A thicker AFL could extend reactive zones, which consequently reduces the activation polarization. However, the fine structure in AFL also brings significant resistance towards fuel transport. The consequent increase in polarization resistance even offsets the benefits from extended TPB and leads to decreased performances. As shown in the figure, the overall polarization ASR of sample ER3 is 0.52 Ω $cm^{-2}$, which displays an increment by 25% compared with the dual-layer counterpart (0.41 Ω $cm^{-2}$). Therefore, an AFL thickness ranging between 17 and 33 μm in this study has been found to enhance the cell performances, which is around 6–11.5% of total anode thickness.

## 4. Conclusion

A series of triple-layer hollow fibres with different AFL thicknesses have been fabricated via a phase-inversion assisted co-extrusion/co-sintering technique, which dramatically simplifies

the preparation process with great control over structures of each layer. Precise control over thicknesses has been achieved by adjusting the extrusion rates during co-extrusion so the effects of AFL thickness on different physical and electrochemical properties could be studied for more efficient cells. SEM images display a typical asymmetric structure, including finger-like channels and sponge-like structure. Inserting an AFL effectively improves both the cell robustness and gas-tightness of the electrolyte layer. In terms of cell performance, there exists a balance between enlarging TPB and introducing more mass transport resistance with increased AFL thickness. AFL between 17 and 33 μm (6–11.5% of total anode thickness) contributes to improved cell performance in this study, and the maximum power density of up to 1.21 W $cm^{-2}$ is obtained at 600 °C using pure $H_2$.

## References


[1] N.Q. Minh, T. Takahashi, Science and Technology of Ceramic Fuel Cells, Elsevier Science, Oxford, UK, 1995.
[2] S.C. Singhal, K. Kendall, W. Winkler, in: S.C. Singhal, Hendall (Eds.), High Temperature Solid Oxide Fuel Cells: Fundamentals, Designs and Applications, Elsevier Oxford, UK, 2003.
[3] R.M. Ormerod, Chem. Soc. Rev. 32 (2003) 17–28.
[4] K. Kendall, Int. J. Appl. Ceram. Technol. 7 (2010) 1–9.
[5] K. Kendall, in: JFCC International Workshop on Fine Ceramics, Elsevier, Nagoya, 1992, pp. 143–148.
[6] B.C.H. Steele, A. Heinzel, Nature 414 (2001) 345–352.
[7] D.J.L. Brett, A. Atkinson, N.P. Brandon, S.J. Skinner, Chem. Soc. Rev. 37 (2008) 1568.
[8] W. Henne, G. Dunweg, W. Schmitz, R. Pohle, F. Lawitzki, US Patent 4164437 (1979).
[9] D. Li, T.-S. Chung, R. Wang, J. Membr. Sci. 243 (2004) 155–175.
[10] J. de Jong, N.E. Benes, G.H. Koops, M. Wessling, J. Membr. Sci. 239 (2004) 265–269.
[11] M.H.D. Othman, Z. Wu, N. Droushiotis, U. Doraswami, G. Kelsall, K. Li, J. Membr. Sci. 351 (2010) 196–204.
[12] M.H.D. Othman, N. Droushiotis, Z. Wu, K. Kanawka, G. Kelsall, K. Li, J. Membr. Sci. 365 (2010) 382–388.
[13] Z. Liang, S. Blackburn, Br. Ceram. Trans. 58 (1998) 113–116.
[14] J.-J. Sun, Y.-H. Koh, W.-Y. Choi, H.-E. Kim, J. Am. Ceram. Soc. 89 (2006) 1713–1716.
[15] N. Droushiotis, M.H.D. Othman, U. Doraswami, Z. Wu, G. Kelsall, K. Li, Electrochem. Commun. 11 (2009) 1799–1802.
[16] T. Li, Z. Wu, K. Li, J. Membr. Sci. 449 (2014) 1–8.
[17] A.V. Virkar, J. Chen, C.W. Tanner, J.-W. Kim, Solid State Ionics 131 (2000) 189–198.
[18] A.C. Müller, D. Herbstritt, E. Ivers-Tiffée, Solid State Ionics 152–153 (2002) 537–542.
[19] K. Chen, X. Chen, Z. Lu, N. Ai, X. Huang, W. Su, Electrochim. Acta 53 (2008) 7825–7830.
[20] M.H.D. Othman, N. Droushiotis, Z. Wu, G. Kelsall, K. Li, Adv. Mater. 23 (2011) 2480–2483.
[21] S. Liu, Ceram. Int. 29 (2003) 875–881.
[22] Xiaoyao Tan, Yutie Liu, K. Li, AIChE J. 51 (2005) 1991–2000.
[23] M.H.D. Othman, Z. Wu, N. Droushiotis, G. Kelsall, K. Li, J. Membr. Sci. 360 (2010) 410–417.
[24] K. Li, J. Kong, X. Tan, Chem. Eng. Sci. 55 (2000) 5579–5588.
[25] C. Yang, W. Li, S. Zhang, L. Bi, R. Peng, C. Chen, W. Liu, J. Power Sources 187 (2009) 90–92.
[26] U. Doraswami, Imperial College London, (Ph.D. thesis), (2010).
[27] Y.-W. Sin, K. Galloway, B. Roy, N.M. Sammes, J.-H. Song, T. Suzuki, M. Awano, Int. J. Hydrogen Energy 36 (2011) 1882–1889.
[28] Z. Wang, N. Zhang, J. Qiao, K. Sun, P. Xu, Electrochem. Commun. 11 (2009) 1120–1123.